

# Hydrogenation driven formation of local magnetic moments in $\text{FeO}_2\text{H}_x$

Alexey O. Shorikov,<sup>1,2,\*</sup> Alexander I. Poteryaev,<sup>1</sup> Vladimir I. Anisimov,<sup>1,2</sup> and Sergey V. Streltsov<sup>1,2</sup>

<sup>1</sup>*M.N. Miheev Institute of Metal Physics of Ural Branch of Russian Academy of Sciences - 620990 Yekaterinburg, Russia*

<sup>2</sup>*Department of theoretical physics and applied mathematics,  
Ural Federal University, Mira St. 19, 620002 Yekaterinburg, Russia*

(Dated: July 11, 2018)

The electronic and magnetic properties of recently discovered new important constituent of the Earth's lower mantle  $\text{FeO}_2\text{H}$  were investigated by means of the density functional theory combined with the dynamical mean field theory (DFT+DMFT). Addition of the hydrogen to the parent  $\text{FeO}_2$  compound, which is an uncorrelated bad metal, destroys the most important ingredient of its electronic structure - O-O molecular orbitals. In effect physical properties of  $\text{FeO}_2$  and  $\text{FeO}_2\text{H}$  turn to be completely different,  $\text{FeO}_2\text{H}$  is a correlated metal with a mass renormalization,  $m^*/m \sim 1.7$ , and magnetic moments on Fe ions become localized with the Curie-Weiss type of uniform magnetic susceptibility.

PACS numbers: 71.27.+a, 71.20.-b, 71.15.Mb, 61.50.Ks, 62.50.-p

Iron oxides are the most important constituents of the Earth's mantle and core. This is the reason why a lot of activity is concentrated on an investigation of their physical and chemical properties under high pressure. Recent discovery of  $\text{FeO}_2$  revised considerably this field<sup>1</sup>. First of all, this compound was not known before 2016 and appears to be the most stable Fe oxide at pressure  $>100$  GPa from the DFT point of view<sup>1</sup>. Second, in contrast to other Fe oxides, which regarded as correlated materials with different type of transitions (metal-insulator, meta-magnetic, spin-state transitions, etc.), Coulomb correlations were found to be almost unimportant in the iron dioxide<sup>2</sup>. There are oxygen "dimers"<sup>30</sup> in  $\text{FeO}_2$  crystal structure, see Fig. 1 (a), and molecular-orbitals due to these "dimers" determine electronic and magnetic properties of this compound. These antibonding O-O molecular-orbitals appear exactly in the same energy region, where Fe  $t_{2g}$  bands are located, hybridize with them and this results in a formation of a pseudogap at the Fermi energy. In effect  $\text{FeO}_2$  is an uncorrelated bad metal<sup>2</sup>.

However, in addition to pure  $\text{FeO}_2$  there may exist hydrate  $\text{FeO}_2\text{H}$  at the Earth's lower mantle conditions<sup>3</sup>. Simple GGA+U calculations showed that  $\text{FeO}_2\text{H}$  is more stable than  $\text{FeO}_2$  and  $\text{H}_2$  separately<sup>3</sup>. The hydrogenation of  $\text{FeO}_2$  was then approved by independent experiments at pressures 100–150 GPa<sup>4</sup> and resulting  $\text{FeO}_2\text{H}$  is now considered as one of the candidates, which forms a so-called  $D''$  layer – a core-mantle boundary<sup>5,6</sup>.

In spite of such a tremendous progress in study of the Earth's lower mantle, physical properties of  $\text{FeO}_2\text{H}$  remain mostly unexplored. In this Report we study electronic and magnetic properties of  $\text{FeO}_2\text{H}$  using calculations performed within the density functional (DFT) and dynamical mean-field (DMFT) theories and show that they are qualitatively different from the pure  $\text{FeO}_2$ . The hydrogenation makes  $\text{FeO}_2$  a correlated material with local magnetic moments.

We start with simple DFT calculations, which give a fully relaxed (atomic positions, volume, and shape) crys-

tal structure for an arbitrary pressure and allows one to study uncorrelated electronic structure of  $\text{FeO}_2\text{H}$ . The pseudo-potential VASP package<sup>7</sup> and generalized gradient approximation (GGA)<sup>8</sup> was utilized. Cutoff energy was set to 1000 eV,  $\mathbf{k}$ -mesh consists of 343 points in the irreducible part of the Brillouin zone. For most of the DFT-based calculations (if not stated specially) the pressure was chosen to be 119 GPa, that corresponds to known experimental crystal structure of  $\text{FeO}_2\text{H}$ <sup>3</sup>.

Fig. 1 shows crystal structures for  $\text{FeO}_2$  and  $\text{FeO}_2\text{H}$  and their corresponding density of states (DOS). In pure

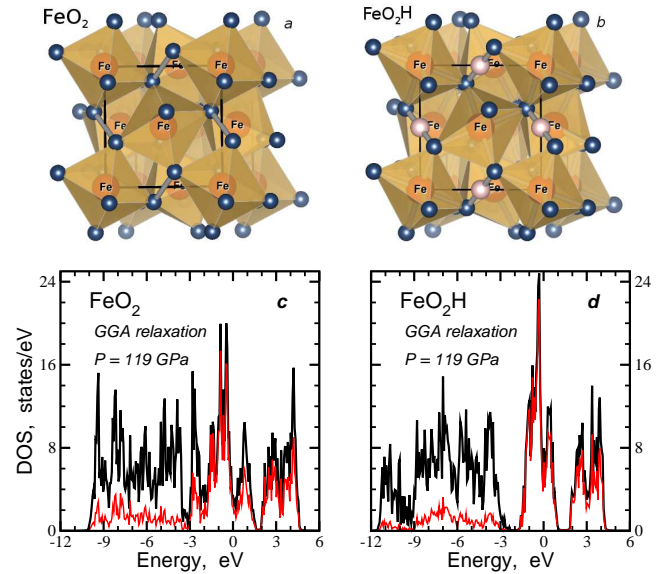


Figure 1: (Color online) Crystal structure for  $\text{FeO}_2$  (a) and  $\text{FeO}_2\text{H}$  (b) as obtained in the GGA relaxation at  $P=119$  GPa. Fe, O, and H atoms are shown by orange, blue, and rose colors, respectively. Short O-O "dimers" that participate in forming antibonding  $\sigma$  O-O molecular-orbitals are shown in gray. Corresponding total (black) and Fe 3d (red) density of states for presented crystal structures are plotted below (c and d).

FeO<sub>2</sub> octahedra are trigonally distorted with the same Fe-O distances,  $d_{Fe-O}=1.75$  Å (all the numbers in this and next paragraph correspond to the crystal structures obtained in the GGA calculations at  $P = 119$  GPa). The distance between two oxygen atoms forming “dimers” (shown by gray color in Fig. 1) is  $d_{O-O}^{dim} = 1.99$  Å. This is much smaller than the length of O-O bonds forming edges of the FeO<sub>6</sub> octahedra ( $d'_{O-O}=2.60$  Å and  $d''_{O-O}=2.33$  Å), but still larger than the distance between oxygen ions in molecular oxygen, which is 1.21 Å. The presence of oxygen “dimers” leads to a formation of O-O molecular-orbitals and substantial modification of FeO<sub>2</sub> electronic structure with respect to other iron oxides. If one imagines “undimerized” iron dioxide with the standard oxidation, an electron counting would give Fe<sup>4+</sup> and (O<sub>2</sub>)<sup>4-</sup>. Similar to the case of pyrite, FeS<sub>2</sub>, strong bonding-antibonding splitting in ligand-ligand “dimers” shifts antibonding  $\sigma$  states upwards and reduces the oxidation of ligand’s complex: (S<sub>2</sub>)<sup>2-</sup> in iron disulfide and (O<sub>2</sub>)<sup>3-</sup> in iron dioxide. The difference between pyrite and iron dioxide is in the strength of this bonding-antibonding splitting, which puts oxygen  $\sigma$ -antibonding bands exactly at the energy position of the Fe  $t_{2g}$  bands, which results in further splitting and unusual valence of Fe:  $3+^{2-}$ .

The corner-shared octahedra of FeO<sub>2</sub> are packed in such way that there are relatively large voids in between. These empty spaces are occupied by the hydrogen in case of FeO<sub>2</sub>H and it is crucial that H sits exactly in a middle of the oxygen “dimers”. The most important structural consequences according to the GGA calculations are (i) approximately 10% increase of the unit cell volume, from  $V_{FeO_2}=76.21$  Å<sup>3</sup> to  $V_{FeO_2H}=83.06$  Å<sup>3</sup>, and (ii) increase of the distance in oxygen “dimers” to  $d_{O-O}^{dim} = 2.27$  Å<sup>31</sup>. The Fe-O and O-O distances in the FeO<sub>6</sub> octahedra are nearly the same as in pure FeO<sub>2</sub>:  $d_{Fe-O}=1.79$  Å,  $d'_{O-O}=2.69$  Å and  $d''_{O-O}=2.36$  Å.

Influence of the hydrogenation of FeO<sub>2</sub> on the electronic structure is more dramatic. It can be traced from the lower part of Fig. 1, where total and partial Fe 3d DOS for both compounds (at the same pressure) are compared. The overall DOSes look very similar accounting for a band narrowing in case of FeO<sub>2</sub>H. As we have pointed out this band narrowing comes from a huge volume enlargement: the unit cell volume of FeO<sub>2</sub>H increases on ~10% with respect to FeO<sub>2</sub>. Hence, the Fe  $t_{2g}$  bands shrink from 4.7 eV in FeO<sub>2</sub> to 2.6 eV in FeO<sub>2</sub>H. The crystal field splitting between  $t_{2g}$  and  $e_g$  orbitals, that are centered around 3 eV, is also affected by volume change and it is reduced from 4.07 eV to 3.46 eV<sup>32</sup>. Nevertheless, this is not the most important change of the band structure. A careful checkup of the bands crossing the Fermi level shows that in the pure FeO<sub>2</sub> there is a strong hybridization of the Fe  $t_{2g}$  states with oxygen orbitals, which form  $\sigma$ -antibonding state in this energy region<sup>2</sup> (the oxygen states can be seen in Fig. 1 as a difference between total and Fe 3d DOSes). In case of FeO<sub>2</sub>H these molecular orbitals are destroyed by the hy-

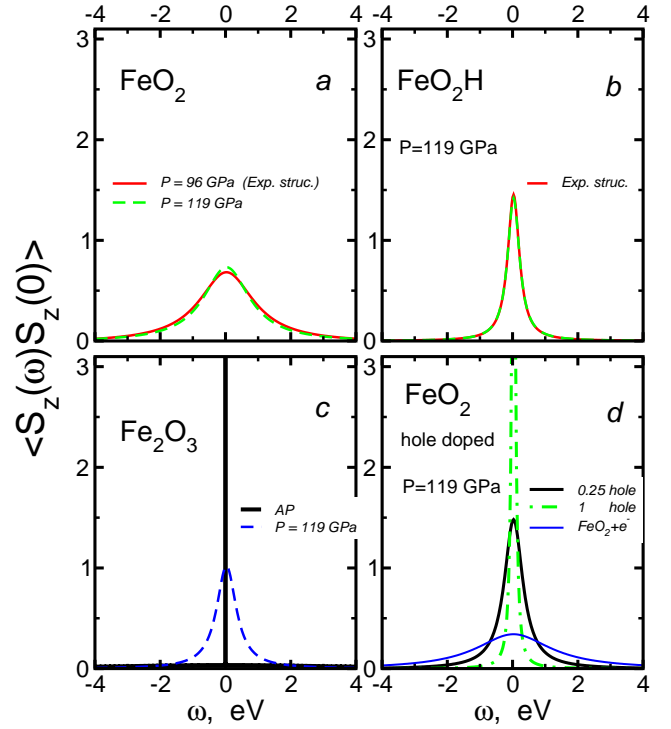


Figure 2: (Color online) Local spin-spin correlation functions obtained within the DFT+DMFT formalism for FeO<sub>2</sub>, FeO<sub>2</sub>H, Fe<sub>2</sub>O<sub>3</sub>, and hole doped FeO<sub>2</sub> ( $T=1160$  K). For details see legends and text.

drogen, and therefore, the hybridization with oxygen in this energy range is extremely small. In effect the bands on the Fermi level are of pure  $t_{2g}$  character as in many other iron oxides.

Thus, already on the DFT level one may argue that iron in FeO<sub>2</sub>H behaves in a conventional way (no molecular-orbitals and effects related to them) and should adopt “3+” valence state, as usual electron counting would suggest. In FeO<sub>2</sub> the valence of iron is the same, “3+”, but this is a consequence of a specific band structure, presence of a strong bonding-antibonding splitting as it was explained in Ref. 2. The fact that the Fe valence is the same in FeO<sub>2</sub> and FeO<sub>2</sub>H is seen from nearly equal Fe-O bond distances obtained in the GGA calculations for these two compounds.

To proceed further with the magnetic properties investigation of compounds of interest we will use the DFT+DMFT method<sup>9,10</sup> as implemented in the AMULET code<sup>20</sup>. This technique is very powerful at studying magnetic properties of materials in a paramagnetic state<sup>11</sup>. Another profit is to be able to make calculations for FeO<sub>2</sub>H, which is a correlated metal with localized magnetic moments, as we will show later. Thus, all compounds will be examined within the same framework regardless correlation strength.

In order to construct noninteracting GGA Hamiltonian, which included the Fe 3d and O 2p states, we use Quantum ESPRESSO<sup>17</sup> and the Wannier function

projection procedure<sup>18</sup>. The effective impurity problem was solved by the hybridization expansion (segment version) Continuous-Time Quantum Monte-Carlo method (CT-QMC)<sup>19</sup>. To reduce off-diagonal elements of the hybridization function a transformation to a local coordinate system is performed by a diagonalization of the corresponding Fe 3d blocks of the Hamiltonian,  $[\sum_{\vec{k}} H(\vec{k})]_{Fe3d}$ . In this case the off-diagonal elements of the hybridization function is less than 5 per cent its diagonal counterparts. We used the same set of Coulomb parameters for all the structures and pressures under investigation,  $U = 6$  eV and  $J_H = 0.89$  eV<sup>2</sup>. In order to avoid double counting of electron-electron interaction in the DFT+DMFT scheme, we use a self-consistent versions of fully localized limit (FLL)<sup>23</sup> for the most of calculations. To benchmark correctness of our results with respect to a choice of double counting we carried out the calculations of the uniform magnetic susceptibility of FeO<sub>2</sub>H using an around mean field (AMF) correction<sup>23</sup>.

Local spin-spin correlation functions,  $\langle \hat{S}_z(\omega) \hat{S}_z(0) \rangle$ , as obtained in the DFT+DMFT calculations, for different compounds are shown in Fig. 2.  $\hat{S}_z = \sum_m (\hat{n}_m^\uparrow - \hat{n}_m^\downarrow)/2$ , where  $\hat{n}_m^\sigma$  is an occupation operator for orbital  $m$  and spin  $\sigma$ . The width of this correlator is inverse proportional to the lifetime of spin moment. It is rather instructive to compare spin-spin correlation functions for FeO<sub>2</sub> and FeO<sub>2</sub>H shown in Fig. 2a-b. The hydrogenation sharp peak and increases its value by factor of 2 approximately. Thus, one may see a dramatic increase of the spin localization in FeO<sub>2</sub>H.

It is tempting to ascribe increase of the spin localization in FeO<sub>2</sub>H to the volume enlargement. However, analysis of the volume dependence of the local spin-spin correlation function shows that this is not the case. One can see from Fig. 2a and Tab. I that there is only a minor change in the width of the correlator for FeO<sub>2</sub> going from  $P = 96$  to 119 GPa, while corresponding change of the volume is  $\sim 9\%$ . It should be noted here that the unit cell volume of FeO<sub>2</sub>H at  $P = 119$  GPa is comparable with the volume of FeO<sub>2</sub> at  $P = 96$  GPa. This validates our assumption that change of volume plays a secondary role in explaining electronic and magnetic properties of FeO<sub>2</sub> and FeO<sub>2</sub>H. Moreover, as one can see from Fig. 2d the electron doping going from FeO<sub>2</sub> to FeO<sub>2</sub>H leads to an opposite effect: decrease of the spin localization (see also discussion about different types of doping below). Thus, one might expect that the main reason of formation of the localized magnetic moments in FeO<sub>2</sub>H is a destruction of the O-O “dimers”. But how localized these moments are?

In order to answer this question we compare FeO<sub>2</sub>H with Fe<sub>2</sub>O<sub>3</sub>, where Fe is also 3+ (see Fig. 2c). At ambient conditions this material is an insulator. Fe<sup>3+</sup> ions are in the high-spin state with well developed local magnetic moments<sup>28</sup>. This can be clearly seen from extremely sharp and strong peak in the correlation function and value of an instant squared magnetic moment,  $\langle m_z^2 \rangle = 21.25 \mu_B^2$ , shown in Tab. I. Albeit  $R\bar{3}c$  phase of Fe<sub>2</sub>O<sub>3</sub>

Table I: Unit cell volumes (third column) obtained at pressures shown in the second column by a full structural relaxation within the GGA method for various compounds (first column). In case of experimental structures the corresponding reference data were used. Instant squared magnetic moments calculated in the DFT+DMFT approach at  $T = 1160$  K are shown in the fourth column.

Compound	P, GPa	V, Å <sup>3</sup>	$\langle m_z^2 \rangle, \mu_B^2$
FeO <sub>2</sub> (exp.) <sup>1</sup>	96	83.00	2.35
FeO <sub>2</sub>	119	76.21	2.45
FeO <sub>2</sub> +0.25 hole	119	76.21	2.89
FeO <sub>2</sub> H (exp.) <sup>3</sup>	119	83.03	2.26
FeO <sub>2</sub> H	119	83.06	2.26
Fe <sub>2</sub> O <sub>3</sub>	AP	100.62	21.25
Fe <sub>2</sub> O <sub>3</sub>	119	67.60	2.19

used in the calculations does not exist above  $P > 30$  GPa at  $T \sim 1000$  K, it is useful to study a degree of the spin localization in a hypothetical structure under pressures, where FeO<sub>2</sub> and FeO<sub>2</sub>H can be formed. At  $P = 119$  GPa a volume of Fe<sub>2</sub>O<sub>3</sub> decreases by 30%,<sup>33</sup> electronic bands become much broader that leads to a metallicity, and as a result, to the broadening of spin-spin correlation function. The instant squared magnetic moment decreases one order in magnitude down to  $\langle m_z^2 \rangle = 2.19 \mu_B^2$  because of a transition from high-spin to low-spin state. Comparing Fig. 2 b and c one may see that the spins in FeO<sub>2</sub>H turn out to be even more localized than in Fe<sub>2</sub>O<sub>3</sub> at the same pressure. Certainly, the appearance of the hydrogen leads to the formation of the local magnetic moments in FeO<sub>2</sub>H.

It is worthwhile mentioning that the hydrogenation resembles hole doping of FeO<sub>2</sub>. Hydrogenating FeO<sub>2</sub> we add one electron to the system. Then the Fermi level should go to the right, crosses the pseudogap and then antibonding O-O band starts occupy (this would spins even less localized). In fact, both the DFT (Fig. 1) and DFT+DMFT (Fig. 4) calculations demonstrate just an opposite behaviour: the Fermi level goes to the left and resides somewhere in the Fe  $t_{2g}$  band. Adding hydrogen to FeO<sub>2</sub> we completely reconstruct electronic structure (break O-O molecular orbitals) and in some sense hydrogenation results in hole, not electron doping of FeO<sub>2</sub> (one may call it “hole-doping-by-electron-doping”). Corresponding spin-spin correlation functions of hole doped FeO<sub>2</sub> and FeO<sub>2</sub>H are indeed rather similar, see Fig. 2 b and d. Thus, both the hydrogenation and hole doping of FeO<sub>2</sub> leads to a formation of localized magnetic moments.

Uniform magnetic susceptibilities,  $\chi(T)$ , of FeO<sub>2</sub>H and Fe<sub>2</sub>O<sub>3</sub> are presented in Fig. 3. They strictly follow Curie-Weiss law typical for systems with localized magnetic moments. Our calculations of the uniform magnetic susceptibilities for FeO<sub>2</sub>H show that the obtained results are robust to the choice of the double counting, with the es-

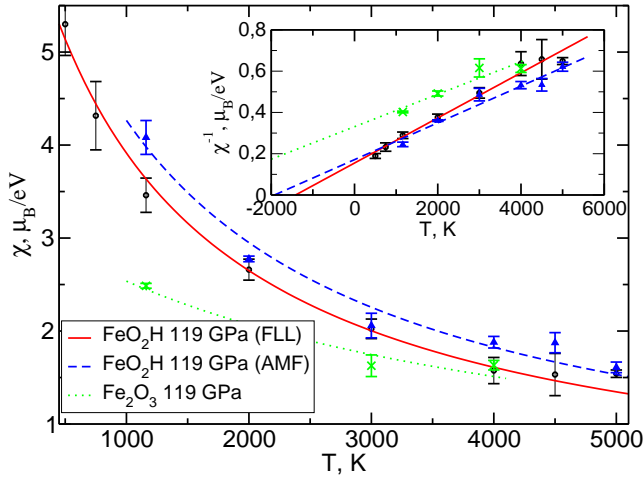


Figure 3: (Color online) Uniform magnetic susceptibility,  $\chi(T)$ , obtained by the DFT+DMFT method for  $\text{FeO}_2\text{H}$  (calculated using different types of the double counting, see text for details) and hypothetical  $\text{Fe}_2\text{O}_3$  under the same pressure of 119 GPa. Inset shows an inverse  $\chi(T)$ .

timated Curie-Weiss temperature to be  $\Theta \sim -1500$  K ( $\Theta \sim -1920$  K) for the FLL (AMF) scheme. This indicates substantial antiferromagnetic exchange interaction in  $\text{FeO}_2\text{H}$ .  $\chi(T)$  of  $\text{FeO}_2\text{H}$ , calculated for different types of double counting, lie above its  $\text{Fe}_2\text{O}_3$  counterpart, that confirms additionally the localized nature of magnetic moments in  $\text{FeO}_2\text{H}$ . In contrast, the uniform magnetic susceptibility of  $\text{FeO}_2$  grows with temperature<sup>2</sup>. The later behavior can be explained by the band structure peculiarities and  $\text{FeO}_2$  should rather be considered as a material, which magnetic properties are described by band magnetism.

It has to be mentioned that while because of the large covalency<sup>2</sup> there is no real difference in occupation numbers for  $\text{FeO}_2$  and  $\text{FeO}_2\text{H}$ , both close six (6.2 electrons for  $\text{FeO}_2$  and 5.7 electrons for  $\text{FeO}_2\text{H}$ ), the influence of hydrogenation can be easily tracked down by investigating the DFT+DMFT spectral functions of  $\text{FeO}_2$  and  $\text{FeO}_2\text{H}$  shown in Fig. 4. We again start with  $\text{FeO}_2$ . The shape of the DFT+DMFT spectral function in  $\text{FeO}_2$  remains almost unchanged with respect to DFT: the original DFT spectra become slightly smoothed by temperature and negligibly narrowed (see inset of Fig. 4 and Ref. 2 for details). This uncorrelated or band-like behavior comes from the fact that the Fermi level is in the pseudogap formed by the  $\text{Fe } t_{2g}$  and mixture of  $\text{Fe } t_{2g}$  and O-O antibonding states. Hence,  $\text{FeO}_2$  is a bad metal with the band-type of magnetism.  $\text{FeO}_2\text{H}$  demonstrates a completely different behavior. The effective mass enhancement,  $m^*/m$ , is 1.7 for  $t_{2g}$  manifold and 1.3 for  $e_g$  orbitals, which is comparable with values for classical Mott systems<sup>29</sup>. Such a renormalization of the spectral weight leads to a quasiparticle peak narrowing in the vicinity of the Fermi level. One may argue that increased role of cor-

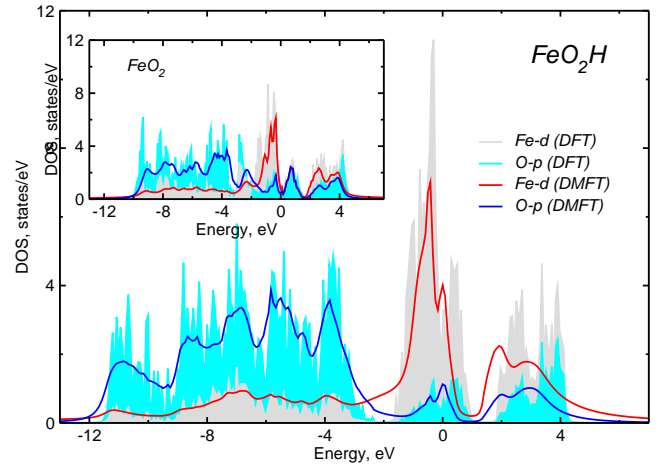


Figure 4: (Color online) Spectral functions for  $\text{FeO}_2\text{H}$  and  $\text{FeO}_2$  (inset). The DFT DOS are shown by filled gray (Fe) and cyan (O) colors. The DFT+DMFT spectral functions for  $T = 1160$  K are shown in red (Fe) and blue (O).

relation effects is due to following factors: *i*) addition of hydrogen destroys oxygen “dimers” and effectively makes a hole doping of the  $\text{Fe } t_{2g}$  subbands, *ii*) reduced  $\text{Fe } t_{2g}$  bandwidth increases  $U/W$  ratio and moves  $\text{FeO}_2\text{H}$  to a more correlated regime.

Summarizing, we have studied the electronic and magnetic properties of  $\text{FeO}_2\text{H}$  by means of the DFT+DMFT method. We have found that hydrogenation changes drastically properties of the parent material. Hydrogen enlarges the volume of the unit cell by almost 10% and, what is more important, destroys O-O “dimers” present in a pure  $\text{FeO}_2$ . In effect the Fermi level is moved from the pseudogap (in  $\text{FeO}_2$ ) to the  $\text{Fe } t_{2g}$  band, and  $\text{FeO}_2\text{H}$  turns out to be a correlated metal ( $m^*/m \sim 1.7$ ) with a sharp quasiparticle peak at the Fermi level and well-formed local magnetic moments, while  $\text{FeO}_2$  is bad uncorrelated metal, which magnetic properties can be described by itinerant theory of magnetism. The Fe ion adopts 3+ valency and is in the low-spin state ( $3d^5$ ,  $S = 1/2$ ) at pressures of hundred GPa. Calculation of uniform magnetic susceptibility demonstrates that there is rather strong antiferromagnetic exchange coupling in  $\text{FeO}_2\text{H}$  (Curie-Weiss temperature  $\Theta \sim -1500 - 2000$  K).

Our findings not only reveal a crucial role of hydrogenation on the physical properties of iron dioxide, but also cast doubt on possibility of consistent description of  $\text{FeO}_2$  and  $\text{FeO}_2\text{H}$  in frameworks of the DFT. Neither GGA nor GGA+U approaches seem to be suitable for this, since while it may look like GGA+U is superior to GGA, because it partially takes into account Hubbard correlations, but in fact it breaks molecular-orbitals, which may lead to “overstabilization” of  $\text{FeO}_2\text{H}$  with respect to  $\text{FeO}_2$ . This means that the use of more appropriate methods, like DFT+DMFT, may change previous results on structural and chemical stability of  $\text{FeO}_2\text{H}$ <sup>3</sup>.

S.S. is grateful to D. Khomskii for various useful dis-



cussions on physical properties of FeO<sub>2</sub>. This work was supported by the grant of the Russian Scientific Founda-

tion (project no. 14-22-00004).

- 
- \* Electronic address: shorikov@imp.uran.ru
- <sup>1</sup> Q. Hu *et al.*, Nature **534**, 241–244 (2016).
  - <sup>2</sup> S. V. Streltsov *et al.*, Scientific Reports **7**, 13005 (2017).
  - <sup>3</sup> M. Nishi *et al.*, Nature **547**, 205 (2017).
  - <sup>4</sup> Q. Hu *et al.*, Proc. Natl. Acad. Sci. **114**, 1498 (2017).
  - <sup>5</sup> J. Liu *et al.*, Nature **551**, 494 (2017).
  - <sup>6</sup> H. Mao *et al.*, Natl. Sci. Rev. **1**, (2017).
  - <sup>7</sup> G. Kresse and J. Furthmüller, Physical Review B **54**, 11169 (1996).
  - <sup>8</sup> J.P. Perdew, K. Burke, and M. Ernzerhof, Physical Review Letters **77**, 3865 (1996).
  - <sup>9</sup> V.I. Anisimov *et al.*, Journal of Physics: Condensed Matter **9**, 7359 (1997).
  - <sup>10</sup> A.I. Lichtenstein and M.I. Katsnelson, Phys. Rev. B **57**, 6884 (1997).
  - <sup>11</sup> G. Kotliar *et al.* Rev. Mod. Phys. **78**, 865 (2006).
  - <sup>12</sup> K. Held *et al.*, Physica Status Solidi (b) **243**, 2599 (2006).
  - <sup>13</sup> A. O. Shorikov *et al.*, Physical Review B **82**, 195101 (2010).
  - <sup>14</sup> J. Kuneš *et al.*, Nature Materials **7**, 198 (2008).
  - <sup>15</sup> A.O. Shorikov *et al.*, Physical Review B **92**, 035125 (2015).
  - <sup>16</sup> N.A. Skorikov *et al.*, Journal of Physics: Condensed Matter **27**, 275501 (2015).
  - <sup>17</sup> P. Giannozzi *et al.*, Journal of Physics: Condensed Matter **21**, 395502 (2009).
  - <sup>18</sup> Dm. Korotin *et al.*, The European Physical Journal B **65**, 91 (2008).
  - <sup>19</sup> E. Gull *et al.*, Reviews of Modern Physics **83**, 349 (2011).
  - <sup>20</sup> “AMULET,” <http://amulet-code.org>.
  - <sup>21</sup> A.A. Dyachenko *et al.*, Physical Review B **93**, 245121 (2016).
  - <sup>22</sup> A.V. Ushakov *et al.*, Physical Review B **95**, 205116 (2017).
  - <sup>23</sup> M. Karolak *et al.*, Journal of Electron Spectroscopy and Related Phenomena **181**, 11 (2010).
  - <sup>24</sup> B. Amadon *et al.*, Physical Review Letters **96**, 066402 (2006).
  - <sup>25</sup> The effective mass enhancement is  $m^*/m = 1 - \partial \Re \Sigma(\omega) / \partial \omega|_{\omega \rightarrow 0}$ , where  $\Sigma(\omega)$  stands for analytical continuation of electronic self-energy to the real frequencies axis made by Padé approximation<sup>26</sup>.
  - <sup>26</sup> K. Beach, R. Gooding, and F. Marsiglio, Physical Review B **61**, 5147–5157 (2000).
  - <sup>27</sup> D. Taylor, British Ceramic Transactions and Journal **83** 92-98 (1984)
  - <sup>28</sup> A. Fujimori *et al.*, Phys. Rev. B **34**, 7318 (1986).
  - <sup>29</sup> E. Pavarini *et al.* Phys. Rev. Lett. **92**, 176403 (2004).
  - <sup>30</sup> We put quotas around dimers, since the distance in these pairs of oxygen atoms is still larger than in molecular oxygen.
  - <sup>31</sup> Note that the GGA+U calculations give rather similar values:  $d_{O-O}^{dim} = 2.23 \text{ \AA}$  and  $V_{FeO_2H} = 83.34 \text{ \AA}^3$ .
  - <sup>32</sup> In the octahedral environment, the  $d$  level is split into triple degenerate  $t_{2g}$  and double degenerate  $e_g$  levels. An additional trigonal distortion leads to the splitting of  $t_{2g}$  level into double degenerate  $e_g^\pi$  and  $a_{1g}$  levels (above mentioned cubic  $e_g$  states are named in this case as  $e_g^\sigma$ ). The resulting splittings are  $\Delta_{e_g^\sigma - a_{1g}}^{FeO_2} = 3.97 \text{ eV}$ ,  $\Delta_{a_{1g} - e_g^\pi}^{FeO_2} = 0.15 \text{ eV}$ , and  $\Delta_{e_g^\sigma - a_{1g}}^{FeO_2H} = 3.44 \text{ eV}$ ,  $\Delta_{a_{1g} - e_g^\pi}^{FeO_2H} = 0.03 \text{ eV}$ . The fine details of the band structure are not important for our study, and thus, we keep using  $t_{2g}$ - $e_g$  notation over the text.
  - <sup>33</sup> Hypothetical  $R\bar{3}c$  structure of Fe<sub>2</sub>O<sub>3</sub> was obtained by full structural relaxation within the GGA.